

## Green Synthesised Bismuth Ferrite for PVA-PANI-BFO Polymer-Nanocomposite Membrane: Impacts on Ionic Conductivity with Variation of Relative Humidity

Diptarka Roy,<sup>1</sup> Kamlesh Pandey<sup>2</sup> and Anil Kumar Yadav<sup>1\*</sup>

<sup>1</sup>Advanced Materials Research Laboratory, Department of Physics, Babasaheb Bhimrao Ambedkar University, Lucknow 226025, Uttar Pradesh, India

<sup>2</sup>National Centre of Experimental Mineralogy and Petrology, University of Allahabad, Allahabad 211002, Uttar Pradesh, India

\*Corresponding author: akyadavbbau@gmail.com

Published online: 25 August 2022

To cite this article: Roy, D. et al. (2022). Green synthesised bismuth ferrite for PVA-PANI-BFO polymer-nanocomposite membrane: Impacts on ionic conductivity with variation of relative humidity. *J. Phys. Sci.*, 33(2), 19–44. <https://doi.org/10.21315/jps2022.33.2.2>

To link to this article: <https://doi.org/10.21315/jps2022.33.2.2>

**ABSTRACT:** *Bismuth ferrite (BFO) nanoparticles were synthesised by an environment-friendly process using the moringa oleifera leaf extract. The synthesised BFO nanoparticles were used as nanofiller to synthesise PVA-PANI-BFO polymer-nanocomposite membrane. Also, the PVA-PANI polymer membrane was synthesised for a comparative study purpose between PVA-PANI and PVA-PANI-BFO membranes. Both the polymer and polymer-nanocomposite membranes were synthesised by the solution cast technique. The Green synthesised BFO nanoparticles and the synthesised membranes were characterised by spectroscopic techniques such as X-ray diffraction (XRD), RAMAN and fourier-transform infrared spectroscopy (FTIR). XRD patterns confirm the BiFeO<sub>3</sub> phase of the synthesised BFO nanoparticles, as well as the existence of PVA, PANI and BFO in the membrane. The Raman spectrum for the synthesised nanoparticles exhibits BFO characteristic bands. The bands of polyvinyl alcohol (PVA) and polyaniline (PANI) are also seen for the membranes. FTIR spectrum indicates some phytochemicals as the functional groups in the synthesised BFO nanoparticles. The surface structures of the synthesised membranes were characterised by field emission scanning electron microscopy (FESEM). Ionic conductivities of the synthesised membranes were calculated by estimating bulk resistance of them from Cole-Cole plots that were obtained with the help of an impedance spectrometer. The conductivities of the membranes change with the relative humidity (RH).*

**Keywords:** BFO nanoparticles, green synthesis, PVA-PANI-BFO and PVA-PANI membranes, relative humidity, ionic conductivity

## 1. INTRODUCTION

Ferroc materials reveal a natural switchable internal ordering characteristic that pays great attention to various functional physics and material science applications. Bismuth ferrite (BFO) is a multiferroic material that reveals both the ferromagnetic and ferroelectric properties such that a magneto-electric coupling occurs by which electric polarisation and magnetic field can be exchanged by each other.<sup>1</sup> It can be found in the forms of single crystal, poly-crystal and numerous nanostructures such as rhombohedral, tetragonal structures, etc.<sup>2</sup> The rhombohedral perovskite-type structure with lattice parameter  $a = 3.965\text{\AA}$  and rhombohedral angle  $\alpha = 89.3^\circ\text{--}89.48^\circ$  belongs to the R3c space group.<sup>3</sup> BFO has a lower insulation resistance due to the creation of oxygen vacancies after the reduction of  $\text{Fe}^{3+}$  into  $\text{Fe}^{2+}$ .<sup>4</sup> The small band gap value, adequate thermal stability and consistent nature with time duration make it suitable for gas sensing applications.<sup>5,6</sup> Different synthesis techniques such as hydrothermal method, mechanochemical, co-precipitation, sol-gel, solution combustion method, etc. are mostly used to prepare  $\text{BiFeO}_3$  (BFO) nanoparticles.<sup>7</sup> For the sustainable and stable nanoparticle synthesis process, it is needed to use some environment-friendly, renewable reducing or capping agents, along with accessible nanoparticle redemption facilities after accomplishing the synthesis process.<sup>8</sup> Recently, the environment-compatible green synthesis route has become an attractive field for synthesising various nanoparticles and their novel applications. The biological compounds that act as the reducing or capping agents create noble nanostructural materials.<sup>9</sup> The present study involves BFO nanoparticle synthesis by following the green route using the *Moringa oleifera* L. leaf extract. *Moringa oleifera* L. is a medicinal plant, that was explained in the first century A.D. in *Sushruta Samhita*, which gives evidence about the existence and beneficial utilisation of that plant in India thousands of years ago. Due to innumerable herbal characteristics, this plant has greater scientific importance. The plant's leaf contains many protein compounds, growth components and different phytochemical substances such as alpha-Carotene, beta-carotene, lutein, neoxanthin, violaxanthin, zeaxanthin, xanthophyll, carotenoids, chlorophyll, phenol, phytate, various amino acids: leucine, alanine, isoleucine, lysine, valine, arginine, glutamic acid, methionine, threonine, phenylalanine, aspartic acid, glycine, cystine, proline, serine, histidine, tryptophan, etc.<sup>10</sup> Those phytochemicals can reduce metal ions during the synthesis of BFO nanoparticle by following the green method.

In the present work, the green synthesised BFO nanoparticles are used as nano-filler in the polymer membrane comprising polyvinyl alcohol (PVA) and polyaniline (PANI). PANI is usually a lower expensive conducting polymer

that can remain stable in the open-air environment. This characteristic gets an advantage during its applications in an electrochemical device. However, PANI in pure powder form does not apply to any electronic devices. A uniform solution is prepared by dissolving it in organic solvents like dimethylformamide (DMF), dimethyl sulfoxide (DMSO), Chloroform ( $\text{CHCl}_3$ ), etc.; thereafter, using the solution casting technique, the PANI membrane is prepared.<sup>11</sup> PANI structure is constructed by a weak organic base as the polymer backbone and strong protonic or organic acids like hydrochloric acid or p-toluene sulfonic acid. The emeraldine base represents the base behaviour of PANI, wherein the emeraldine salt shows conductive nature. The PANI (emeraldine base) contains diamine and diimine units. During exposure to the air, the partial oxidation of the base extends the comparative amount of imine units.<sup>12</sup> Delocalisation of  $\pi$  electron at the PANI backbone renders the novel optical and electrical characteristics. This type of conductive polymer consists of very closely spacing molecules that alter the single and double bonds, the result of which electrons move from one terminal to another terminal by the extended p-orbital system.<sup>13</sup> PVA is a semicrystalline material, often used as a host polymer of numerous nanofillers and copolymers to prepare electrolytes of various electrochemical devices. The incorporation of nanoparticles in the polymer matrix affects its configuration; optical and electrical behaviours.<sup>14</sup> Present study has brought into focus a new polymer-nanocomposite system, which consists of PVA, PANI and nanostructural BFO. A solution cast technique is used to prepare polymer membranes. The ionic conductivities of the synthesised membranes that vary with the relative humidity of the ambient are investigated.

## 2. MATERIALS AND EXPERIMENTAL PROCEDURE

### 2.1 Ingredients and Chemicals

PVA (98%–99% hydrolysed, M.W. 98,000 g/mol, Across organics, USA), PANI (Emeraldine base, Alfa Aesar, Thermo Fisher Scientific, USA), N, N-Dimethylformamide (M.W. 73.09 g/mol, MOLYCHEM, India), Bismuth (III) Nitrate Pentahydrate (98%, M.W. 485.07 g/mol, LOBA Chemie, India), Ferric Nitrate Nonahydrate (98%, M.W. 404 g/mol, Thermo Fisher Scientific India Pvt. Ltd, India) were used to synthesise BFO nanoparticles and the polymer membrane where BFO nanoparticles were used as nanofiller. *Moringa oleifera* L. leaves were collected from Babasaheb Bhimrao Ambedkar University campus, Lucknow, India, were used to synthesise BFO nanoparticles. Ethyl alcohol (99.9%) was used to prepare *Moringa oleifera* L. leaf extract. Nitric acid (69.5%, MOLYCHEM, India), Liquor ammonia (25%, M.W. 17.03 g/mol,

Thermo Fisher Scientific India Pvt. Ltd, India), Whatman filter paper No.1 (diameter 125 mm, Cat No. 1001125, GE Healthcare UK Limited, UK) were used during BFO nanoparticle synthesis process.

## 2.2 Green Synthesis of Bismuth Ferrite (BFO) Nanoparticles

### 2.2.1 Preparation of *Moringa oleifera* L. leaf extract

In the beginning, fresh *Moringa oleifera* L. leaves (as shown in Figure 1) were collected and washed well by using double-distilled water, then dried up at room temperature (20°C–22°C). The leaf extract was obtained by keeping 20 g of chopped leaf immersed in 40 mL of ethanol and heated at 60°C for 2 h using a hot plate attached to the magnetic stirrer. Thus, a green-coloured solution was prepared, which after filtration with a Whatman filter paper No. 1, the leaf extract was obtained.

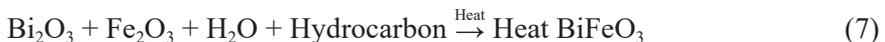
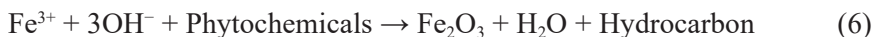


Figure 1: *Moringa oleifera* L. leaves.

### 2.2.2 Synthesis of BFO nanoparticles using *Moringa oleifera* L. leaf extract

To synthesise BFO nanoparticles, initially, 200 mL of 0.1 M ferric nitrate nonahydrate [ $\text{Fe}(\text{NO}_3)_3 \cdot 9\text{H}_2\text{O}$ ] aqueous solution and 200 mL of 0.1 M bismuth nitrate pentahydrate [ $\text{Bi}(\text{NO}_3)_3 \cdot 5\text{H}_2\text{O}$ ] aqueous solution (which contains 15 mL of  $\text{HNO}_3$ ) were prepared. Each of the precursor solutions was prepared with a magnetic stirrer's help after stirring for 6 h. Then both the precursor

solutions were mixed up with each other by constant stirring for another 6 h. After accomplishing the mixing up process, *Moringa oleifera* L. leaf extract was added to the final solution by maintaining the weight to volume ratio (w/v) of the total precursor to the extract at approximately 1:1. Then the solution turned brownish from the almost transparent colour and stirring of the mixture continued for 6 h. Colour changing of the mixture indicated the reduction of metallic ions by the plant metabolites (Carotene, lutein, carotenoids, chlorophyll, phenol, various amino acids, etc.) and the formation of BFO nanoparticles. To get precipitate, 60 mL liquor NH<sub>3</sub> (25%) was mixed in the preceding solution. Then the precipitate was collected with the help of Whatman filter paper No. 1. Also, several impurities were removed while rinsing the collected precipitate by double-distilled water through filtration. After drying the collected precipitate at room temperature, the precipitate was annealed at 600°C for 2 h with the help of a muffle furnace. This temperature is adequate to remove residual components (like hydroxide, nitric acid) and obtain a crystalline pure phase of BFO nanoparticles. Also, at the same temperature, bismuth(III) oxide (Bi<sub>2</sub>O<sub>3</sub>) reacts completely with iron(III) oxide (Fe<sub>2</sub>O<sub>3</sub>) and produces single-phase BFO. The annealed sample was rubbed gently using an Agate mortar-pestle to get the BFO nanoparticles as powder form. A flow chart for synthesising BFO nanoparticles is shown in Figure 2. The plausible reaction mechanisms related to the reduction of Bi<sup>3+</sup> and Fe<sup>3+</sup> ions and the formation of BFO nanoparticles are given below:



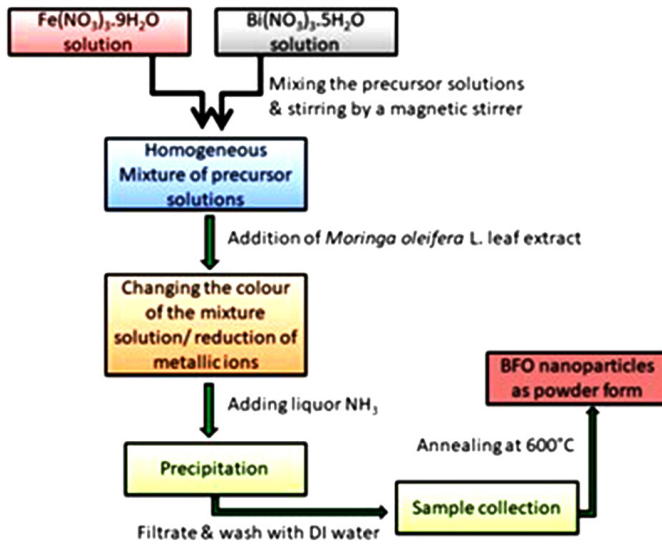


Figure 2: Flow-chart for BFO nanoparticles synthesis.

### 2.3 Synthesis of Composite Polymer Membranes

To prepare the PVA-PANI membrane, the weight percentage of PVA and PANI were taken as 95% and 5%, respectively, in the 100% of total compound. PVA and PANI with the particular amounts were added to 10 mL of DMF solvent separately. PANI in DMF was stirred for 10 hours at room temperature. PVA in DMF was stirred for 4 h at 70°C for dissolution. After that, both the solutions of PVA and PANI were mixed up and stirred at 70°C for 2 h. Then the heating of that mixture was stopped and further stirred for another 2 h to get the PVA-PANI matrix. That mixture solution was poured into a petri dish, then dried through a particular ambient situation.

PVA-PANI-BFO membrane was prepared by adding 2% weight of the synthesised BFO nanoparticles to the 98% weight of PVA-PANI composition, where their ratio (PVA:PANI) was identical to that for before mentioned PVA-PANI membrane. The PVA-PANI matrix was obtained by following the previous process for synthesising the PVA-PANI membrane. The BFO nanoparticles were added to the PVA-PANI matrix and stirred for 2 h. Then the mixture was poured into a petri dish through a particular ambient condition, and after drying the matrix, the composite membrane was prepared.

## 2.4 Characterisation Techniques

The crystallite characteristics of the green synthesised BFO nanoparticles, synthesised PVA-PANI and PVA-PANI-BFO polymer-nanocomposite membranes were characterised by X-ray diffractometer (RIGAKU ULTIMA 4, Japan) with Cu-K $\alpha$  radiation having the wavelength  $\lambda = 0.154$  nm, within the range  $2\theta = 20^\circ$ – $80^\circ$ . The chemical compositions and phase of the synthesised nanomaterials and polymer-nanocomposite membranes were analysed by a Confocal Raman spectrophotometer (UniRAM, Taiwan) with laser sources at 785 nm with variable power in the spectral range ( $100\text{ cm}^{-1}$ – $2000\text{ cm}^{-1}$ ). The existence of functional groups in green synthesised BFO nanoparticles were detected by FTIR with an ATR spectrophotometer (Bruker Alpha, Germany) in the range between  $4000\text{ cm}^{-1}$ – $500\text{ cm}^{-1}$ . The morphological properties of the synthesised different polymer membrane systems were investigated by field emission scanning electron microscopy (FESEM) images (Sigma300, ZEISS, Germany). The electrical conductivities of the synthesised membranes were measured with the help of an impedance spectrometer (HIOKI 3522-50 LCR HITESTER, Japan).

## 2.5 Measurement of the Ionic Conductivities and Weights of the Synthesised Polymer Membranes

The electrical conductivities of the synthesised membranes were measured from the spectral data of an impedance spectrometer (HIOKI 3522-50 LCR HITESTER, frequency range 40 Hz–100 KHz) at different ambient conditions with different humidity. The synthesised PVA-PANI and PVA-PANI-BFO membranes were placed inside non-blocking electrodes that formed an equivalent RC parallel circuit (involves to resistor and capacitor) for the membrane and electrode-membrane interfaces. Ionic conductivity ( $\sigma$ ) of a sample membrane can be estimated by using the following equation:

$$\sigma = \frac{t}{RA} \quad (8)$$

Where,  $R$ ,  $A$  and  $t$  denote the bulk resistance, cross-sectional area and thickness of the polymer or polymer-nanocomposite membrane, respectively.<sup>15,16</sup> The present study investigates the changes in ionic conductivity depending on variable relative humidity conditions for the synthesised PVA-PANI membranes with BFO nanofiller and without BFO nanofiller.

Also, at different relative humidity conditions, the variations of weights due to the adsorption of humidity in the membranes were studied. To study the weight variation with relative humidity, the same initial weights (0.1 g) for the PVA-PANI and PVA-PANI-BFO membranes were recorded at a minimum relative humidity (28%).

### 3. RESULTS AND DISCUSSION

#### 3.1 Characterisations of the Synthesised BFO Nanoparticles and the Synthesised PVA-PANI Polymer Membranes with and without BFO Nanofiller

##### 3.1.1 X-ray diffraction spectroscopy

The X-ray diffraction pattern of the green synthesised BFO nanoparticles is shown in Figure 3. The peak positions are 22.45° (101), 31.98° (012), 39.50° (021), 45.82° (202), 51.54° (113), 57.10° (300), 67.07° (220), 70.66° (015), 71.33° (303) and 75.94° (312). All those peaks are similar to JCPDS card number 00-020-0169. This confirms the formation of BFO.<sup>17</sup> Average crystallite size for the green synthesised BFO nanoparticles is estimated from Debye Scherrer's equation:

$$d = \frac{0.9\lambda}{\beta \cos \theta} \quad (9)$$

Where  $\lambda$  = wavelength of the X-ray radiation,  $\beta$  = the full width at half maximum (FWHM) of the peaks present in the XRD pattern,  $\theta$  = the Bragg's diffraction angle, 0.9 = the factor which depends on the crystalline character of the synthesised material. The shape factor (K) in the Sherrer equation is a dimensionless factor. It varies from 0.89 to 1.04, based on the actual shape of the crystallite.<sup>18</sup> As per previously reported literature, the shape factor for the synthesised BFO is 0.9.<sup>19</sup> The calculated average crystallite size for the green synthesised BFO nanoparticles is 12.3 nm.

The XRD patterns of the PVA-PANI and PVA-PANI-BFO membranes are shown in Figure 4. PVA membrane shows the crystallite peak at 19.50°, also the PANI has the characteristic peaks at 20° and 24°. <sup>20,21</sup> But, after the conjugation of PANI with PVA in the membranes, those peaks are not clearly found for both the PVA-PANI and PVA-PANI-BFO membranes. A sharp peak is seen at 29.60° and 29.37° for PVA-PANI and PVA-PANI-BFO membranes,

respectively, indicating PANI.<sup>22</sup> The peak positions at  $39.49^\circ$  and  $47.42^\circ$  for PVA-PANI membrane, which are found at  $39.85^\circ$  and  $47.22^\circ$  for PVA-PANI-BFO membrane, represent the peaks of highly protonated PVA-PANI composite.<sup>23</sup> For the PVA-PANI-BFO membrane, the peak found near about  $57^\circ$  indicates the existence of BFO nanofiller in the polymer membrane.

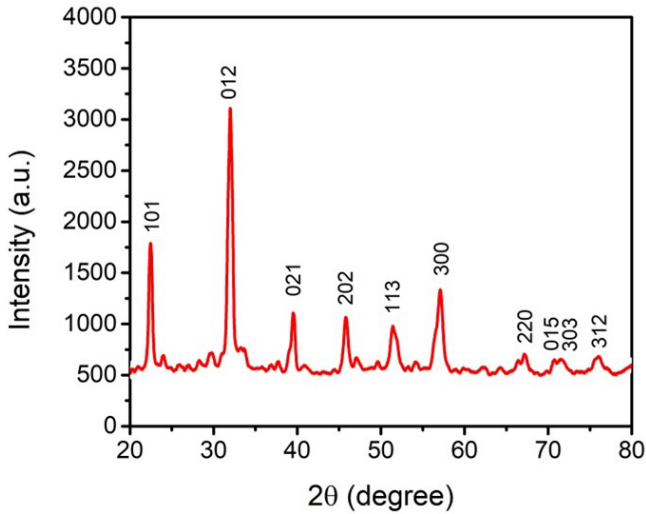


Figure 3: XRD pattern of the green synthesised BFO nanoparticles.

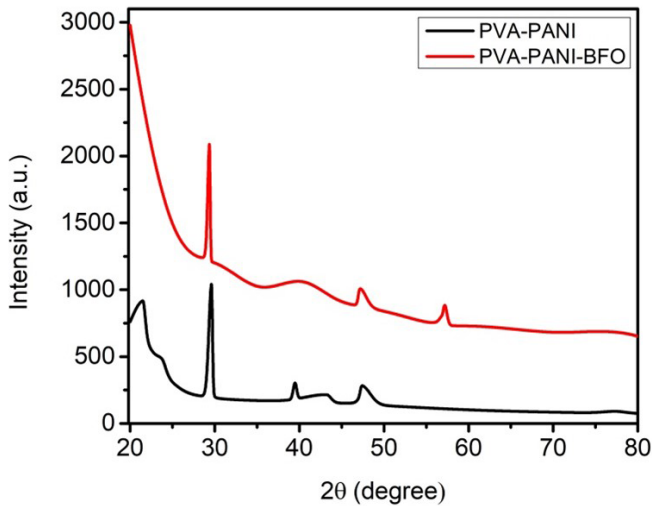


Figure 4: XRD pattern of the synthesised PVA-PANI and PVA-PANI-BFO membranes.

### 3.1.2 Raman Spectroscopy

The Raman spectrum of the green synthesised BFO nanoparticles is presented in Figure 5. The band obtained at  $140\text{ cm}^{-1}$  and  $226\text{ cm}^{-1}$  indicate the characteristic bands of BFO (i.e. the  $A_1$  mode of vibration). The band at  $291\text{ cm}^{-1}$  shows the vibrational E mode of the O atom.<sup>24,25</sup> The band at  $608\text{ cm}^{-1}$  (E mode), is raised owing to the internal stretch of  $\text{FeO}_6$ . The band at  $493\text{ cm}^{-1}$  ( $A_4$  mode), represents the Fe stretching.<sup>26</sup> The band at  $539\text{ cm}^{-1}$  represents the  $A_1$  mode of vibration for BFO. Also, the band at  $407\text{ cm}^{-1}$  indicates the first-order Raman mode of BFO.<sup>27</sup>

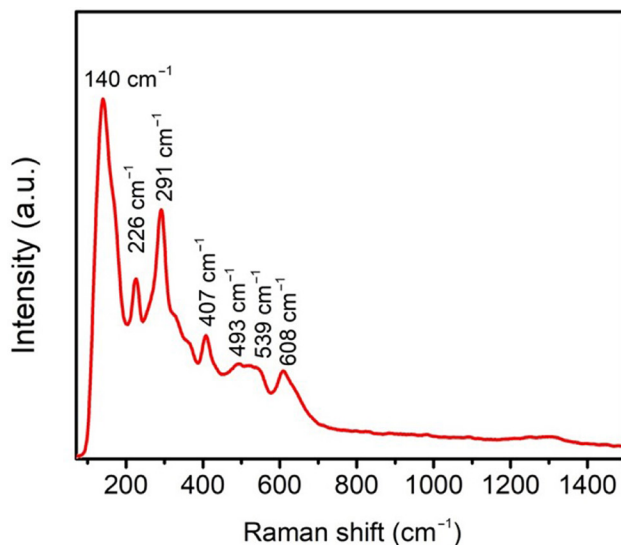


Figure 5: Raman spectrum of the green synthesised BFO nanoparticles.

The Raman spectra for PVA-PANI and PVA-PANI-BFO composite membranes are given in Figure 6. Also, the corresponding optical images of the membranes taken by an optical microscope attached with the Raman spectrometer are shown in Figure 7. The optical images show the homogeneous distribution of the PVA-PANI-BFO membrane compared to the PVA-PANI membrane, which may be due to the favourable interaction of BFO nanoparticles with PVA and PANI in the composite membrane. The band positions for both the cases almost remain the same, and they differ only in intensities. Due to the effect of BFO nanofiller, the PVA-PANI-BFO membrane shows slightly lower intensities in the Raman bands, which are found comparatively higher for the PVA-PANI membrane. Some Raman bands are slightly shifted due to the effect

of BFO nanofiller in the membrane. The percentage ratio of nanofiller to the polymer components in the membrane is minimal; so BFO peaks are not found individually in the PVA-PANI-BFO membrane. The Raman bands at  $831\text{ cm}^{-1}$  (C-H out of plane bend),  $1451\text{ cm}^{-1}$  (C-N<sup>+</sup> stretch for semiquinoid rings),  $1578\text{ cm}^{-1}$  (C=C stretch in quinonoid rings),  $1156\text{ cm}^{-1}$  (C-H in-plane bend of the quinonoid rings),  $1331\text{ cm}^{-1}$  (C-N<sup>+</sup> vibration for the delocalised polaronic structure), respectively are the characteristic bands of PANI.<sup>28–30</sup> The band observed at  $1211\text{ cm}^{-1}$  relates to the C-N stretch for the benzene ring in PANI, also indicates the C-O stretch in PVA. Besides this, the band at  $1451\text{ cm}^{-1}$  is also associated with the CH<sub>2</sub> bending of PVA. PANI as a conducting polymer shows the strongest Raman activities than other components in the synthesised polymer membranes. The characteristic Raman bands of PANI are slightly shifted from the actual positions due to the intermolecular interactions with other components (PVA, BFO).<sup>31</sup> Besides these, the bands at  $417\text{ cm}^{-1}$  and  $523\text{ cm}^{-1}$  define the out-of-plane benzene ring deformation of PANI.<sup>32</sup> The bands at  $742\text{ cm}^{-1}$  and  $779\text{ cm}^{-1}$  (which is relocated to  $775\text{ cm}^{-1}$  for PVA-PANI-BFO membrane) can be assigned by several vibrations of PVA. However, the exact assignments for those bands are not possible to find due to multiple interatomic interactions between different elements in the composite membrane.<sup>33</sup>

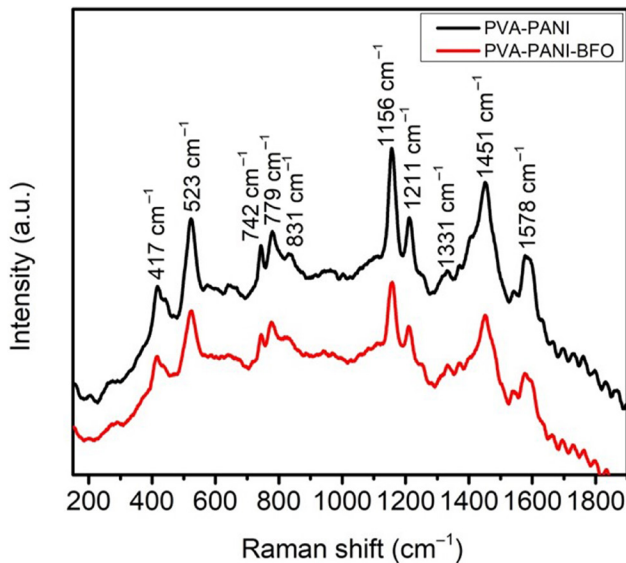


Figure 6: Raman spectra for the PVA-PANI and PVA-PANI-BFO membranes.

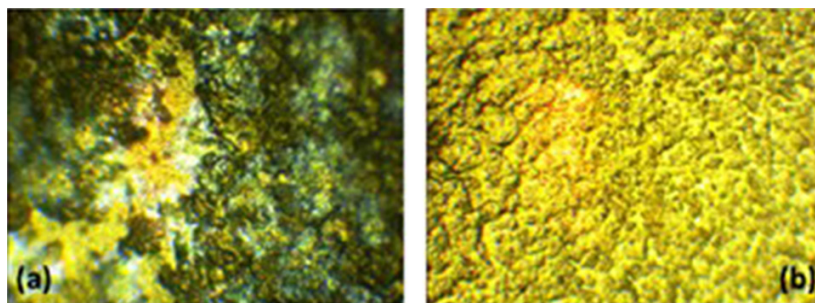


Figure 7: Optical images of: (a) PVA-PANI and (b) PVA-PANI-BFO membranes.

### 3.1.3 FTIR spectroscopy

The FTIR spectra of *Moringa oleifera* L. leaf extract and the green synthesised BFO nanoparticles using it are shown in Figure 8. The *Moringa oleifera* L. leaf extract shows the FTIR peaks at  $3348\text{ cm}^{-1}$ ,  $2975\text{ cm}^{-1}$ ,  $2926\text{ cm}^{-1}$ ,  $1644\text{ cm}^{-1}$ ,  $1509\text{ cm}^{-1}$ ,  $1452\text{ cm}^{-1}$ ,  $1382\text{ cm}^{-1}$ ,  $1271\text{ cm}^{-1}$ ,  $1081\text{ cm}^{-1}$ ,  $1042\text{ cm}^{-1}$  and  $877\text{ cm}^{-1}$ . They indicate the phytochemicals in the leaf extract such as aromatic or aliphatic alcohols, phenols, amine, ketones, esters and some nitrogen-containing compounds that act as the reducing and capping agents during BFO nanoparticles synthesis. The peaks at  $3348\text{ cm}^{-1}$  and  $2926\text{ cm}^{-1}$  are attributed to O-H stretch for the  $-\text{OH}$  group of alcohol and the C-H stretch of the  $-\text{CH}_3$  group in alkane, respectively. The peaks at  $1509\text{ cm}^{-1}$  and  $1452\text{ cm}^{-1}$  represent the C=C stretch of the aromatic group. The peak noticed at  $877\text{ cm}^{-1}$  indicates the C=C functions. Also, the peaks at  $1271\text{ cm}^{-1}$  and  $1081\text{ cm}^{-1}$  that belong to the ranges  $1541\text{ cm}^{-1}$ – $420\text{ cm}^{-1}$  imply the aliphatic or aromatic compounds.<sup>34</sup> The peak at  $1644\text{ cm}^{-1}$  specifies the alkyne (C-C) and carbonyl (C=O) groups.<sup>35</sup> The peaks at  $1382\text{ cm}^{-1}$  and  $2975\text{ cm}^{-1}$  are detected due to N-O stretching from aliphatic nitrogen and C-H stretching of the  $\text{CH}_2$  group in the leaf extract.<sup>36</sup> The peak at  $1042\text{ cm}^{-1}$  indicates polysaccharides.<sup>37</sup>

Among the above-mentioned *Moringa oleifera* L. leaf extract peaks, some are detected in the BFO FTIR spectrum, though they are little shifted in positions. Those peaks positions are  $1642\text{ cm}^{-1}$ ,  $1513\text{ cm}^{-1}$ ,  $1463\text{ cm}^{-1}$ ,  $1104\text{ cm}^{-1}$  and  $859\text{ cm}^{-1}$ , which represent some functional groups for the phytochemicals of the *Moringa oleifera* L. leaf extract in the green synthesised BFO nanoparticles. Also, the peaks at  $985\text{ cm}^{-1}$  and  $926\text{ cm}^{-1}$  are found due to aliphatic or aromatic groups. The peak at  $814\text{ cm}^{-1}$  indicates trapped nitrate ions and may also associate with the Fe-O stretching in BFO. The peak at  $1642\text{ cm}^{-1}$  indicates the H-O-H bend of  $\text{H}_2\text{O}$  that probably comes into the synthesised BFO powder sample from the ambient moisture.<sup>38,39</sup>

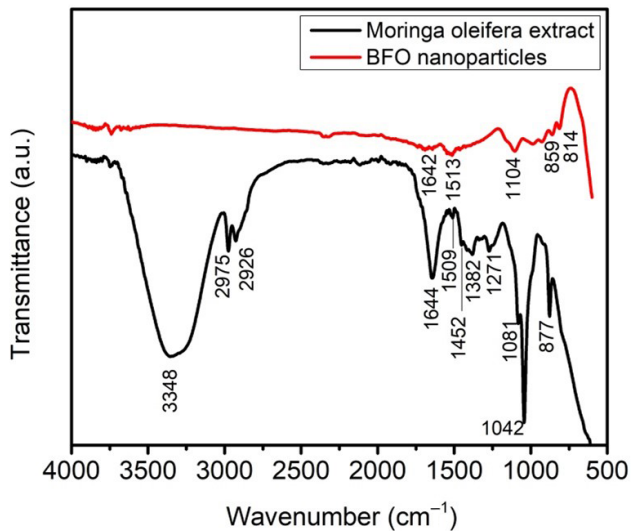


Figure 8: FTIR spectra of *Moringa oleifera* L. leaf extract and BFO nanoparticles.

The FTIR spectra for the PVA-PANI and PVA-PANI-BFO membranes at different relative humidity conditions are represented in Figure 9 and Figure 10, in between the ranges  $500\text{ cm}^{-1}$ – $3000\text{ cm}^{-1}$  and  $3000\text{ cm}^{-1}$ – $4000\text{ cm}^{-1}$ , separately. Peaks for the PVA-PANI membranes are found at  $3293\text{ cm}^{-1}$ ,  $2934\text{ cm}^{-1}$ ,  $2912\text{ cm}^{-1}$ ,  $1734\text{ cm}^{-1}$ ,  $1658\text{ cm}^{-1}$ ,  $1594\text{ cm}^{-1}$ ,  $1564\text{ cm}^{-1}$ ,  $1440\text{ cm}^{-1}$ ,  $1372\text{ cm}^{-1}$ ,  $1324\text{ cm}^{-1}$ ,  $1238\text{ cm}^{-1}$ ,  $1141\text{ cm}^{-1}$ ,  $1088\text{ cm}^{-1}$ ,  $1022\text{ cm}^{-1}$ ,  $944\text{ cm}^{-1}$  and  $840\text{ cm}^{-1}$  at the relative humidity (RH) 28% of the ambient. At the same RH condition, for the PVA-PANI-BFO membrane, some of those peaks remain almost the same, and some are very little shifted in positions, which are  $3294\text{ cm}^{-1}$ ,  $2937\text{ cm}^{-1}$ ,  $2909\text{ cm}^{-1}$ ,  $1734\text{ cm}^{-1}$ ,  $1655\text{ cm}^{-1}$ ,  $1594\text{ cm}^{-1}$ ,  $1561\text{ cm}^{-1}$ ,  $1437\text{ cm}^{-1}$ ,  $1375\text{ cm}^{-1}$ ,  $1321\text{ cm}^{-1}$ ,  $1239\text{ cm}^{-1}$ ,  $1140\text{ cm}^{-1}$ ,  $1090\text{ cm}^{-1}$ ,  $1021\text{ cm}^{-1}$ ,  $944\text{ cm}^{-1}$  and  $836\text{ cm}^{-1}$ , respectively. But some extra peaks are raised at  $1499\text{ cm}^{-1}$ ,  $661\text{ cm}^{-1}$  and  $647\text{ cm}^{-1}$ , which differ from the peaks of the PVA-PANI membrane. They may indicate the crosslinking between PANI and BFO nanoparticles for the formation of PVA-PANI-BFO polymer-nanocomposite membrane. Also, the shifting of peaks indicates the interactions between PVA, PANI and BFO. The peaks found at  $3294\text{ cm}^{-1}$ ,  $2909\text{ cm}^{-1}$ ,  $1655\text{ cm}^{-1}$ ,  $1594\text{ cm}^{-1}$ ,  $1437\text{ cm}^{-1}$ ,  $1321\text{ cm}^{-1}$ ,  $836\text{ cm}^{-1}$  and  $661\text{ cm}^{-1}$  are analogous to the peaks stated previously in Prabhakaran and Hemalatha (2012) for PVA-PANI-BFO polymer nanocomposite.<sup>40</sup> The peaks at  $1594\text{ cm}^{-1}$  and  $1499\text{ cm}^{-1}$  are associated with C=C stretch for quinoid and benzenoid moieties. The peak positions at  $1321\text{ cm}^{-1}$ ,  $1140\text{ cm}^{-1}$  and  $836\text{ cm}^{-1}$  relate to the C-N stretch, C-H in-plane bend, and C-H out of plane bends of PANI. The peaks at  $944\text{ cm}^{-1}$ ,

1021  $\text{cm}^{-1}$  and 1655  $\text{cm}^{-1}$  are the characteristic peaks of PVA, which denote the C-O stretching vibration. The peak at 2937  $\text{cm}^{-1}$  and 2909  $\text{cm}^{-1}$  relates to the asymmetric aromatic C-H stretch, specifies the PANI-BFO interactions in the PVA-PANI-BFO membrane. The peak corresponding to 661  $\text{cm}^{-1}$  indicates the Fe-O vibration of BFO inside the polymer-nanocomposite membrane.<sup>40</sup> Peaks at 1239  $\text{cm}^{-1}$  and 1561  $\text{cm}^{-1}$  represent the typical peaks of PANI that are related to the C-N and C=N stretch.<sup>41</sup> Peak at 647  $\text{cm}^{-1}$  specifies the  $\text{NH}_2$  out of plane bending vibration for aromatic amine.<sup>42</sup> Peaks position 1375  $\text{cm}^{-1}$  and 1090  $\text{cm}^{-1}$  are the usual peaks for PANI.<sup>43</sup> The peaks in between 1400  $\text{cm}^{-1}$ –1460  $\text{cm}^{-1}$  indicate the vibrations of PVA-PANI composition.<sup>44,45</sup> Now any broad peak in between the range 3000  $\text{cm}^{-1}$ –4000  $\text{cm}^{-1}$  directs the peak of  $\text{H}_2\text{O}$ , which is generated owing to the hydrogen bond among the water molecules. Due to higher IR radiation absorption capability by  $\text{H}_2\text{O}$  molecules, that region is not useful to analyse any other chemical groups.<sup>46,47</sup> Thus a broad peak around 3294  $\text{cm}^{-1}$  indicates hydrogen bond interaction due to trapped  $\text{H}_2\text{O}$  molecules in the PVA-PANI and PVA-PANI-BFO membrane from the ambient at different RH conditions. Figure 10 represents the respective broad absorption bands for PVA-PANI and PVA-PANI-BFO membranes at different RH between the ranges 3000  $\text{cm}^{-1}$ –4000  $\text{cm}^{-1}$ , which hints inevitable existence of  $\text{H}_2\text{O}$  in synthesised membranes.<sup>48</sup> It is seen that at RH = 28%, the PVA-PANI membrane shows a broader peak with higher intensity relative to the PVA-PANI-BFO membrane. At RH = 55%, both peaks almost overlap, and at RH = 95%, once again, that peak for the PVA-PANI membrane becomes broader with slightly higher intensity in comparison to the PVA-PANI-BFO membrane. The broader peak with higher intensity signifies the more hydrogen bonding interaction that indicates the absorption of the more  $\text{H}_2\text{O}$  molecules by the membrane. Accordingly, at lower and higher RH (RH = 28% and RH = 95%), the PVA-PANI membrane absorbs larger amounts of moisture from the ambient than the PVA-PANI-BFO membrane. Therefore, PVA-PANI-BFO polymer-nanocomposite membrane is more stable against the RH (at lower and higher RH) of ambient in comparison to the PVA-PANI polymer membrane.

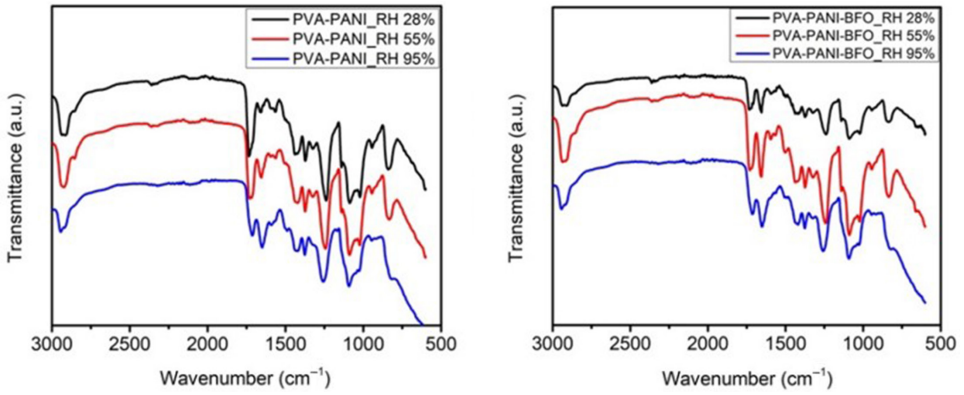


Figure 9: FTIR spectra of the PVA-PANI and PVA-PANI-BFO membranes in the ranges between 500 cm<sup>-1</sup>–3000 cm<sup>-1</sup> at different RH.

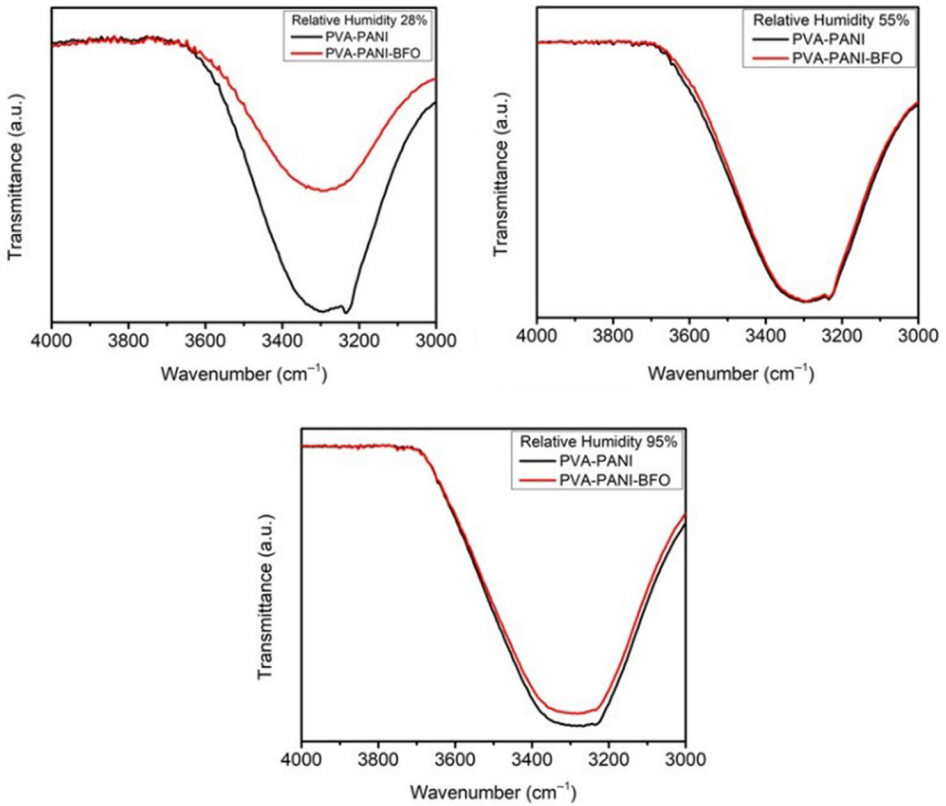


Figure 10: FTIR spectra of the PVA-PANI and PVA-PANI-BFO membranes in between the range 3000 cm<sup>-1</sup>–4000 cm<sup>-1</sup> at different RH.

### 3.1.4 FESEM

The FESEM images for the PVA-PANI polymer membrane and PVA-PANI-BFO polymer-nanocomposite membranes with different magnifications are shown in Figure 11 (a), (b), (c) and (d) separately. A particular systematic arranged surface distribution is seen for the PVA-PANI-BFO membrane relative to the PVA-PANI membrane. The structural growth on the surface of the PVA-PANI-BFO membrane looks like *Tabernaemontana divaricate* flower petals, which is seen in Figure 12. Such unique surface structure is formed by the influence of green synthesised BFO nanoparticles, which act as nanofiller during the synthesis of PVA-PANI-BFO polymer-nanocomposite membrane. Also, many well-ordered grooves can be seen on that surface, which is responsible for the membrane's roughness. The roughness of the surface can improve the hydrophobicity of the membrane.<sup>49</sup> So, the PVA-PANI-BFO membrane is less hydrophilic than the PVA-PANI membrane; that characteristic is reflected on the wide FTIR band within the range  $3000\text{ cm}^{-1}$ – $4000\text{ cm}^{-1}$ , obtained from the respective membranes at lower RH (RH = 28%) and as well as higher RH (RH = 95%) of the ambient.

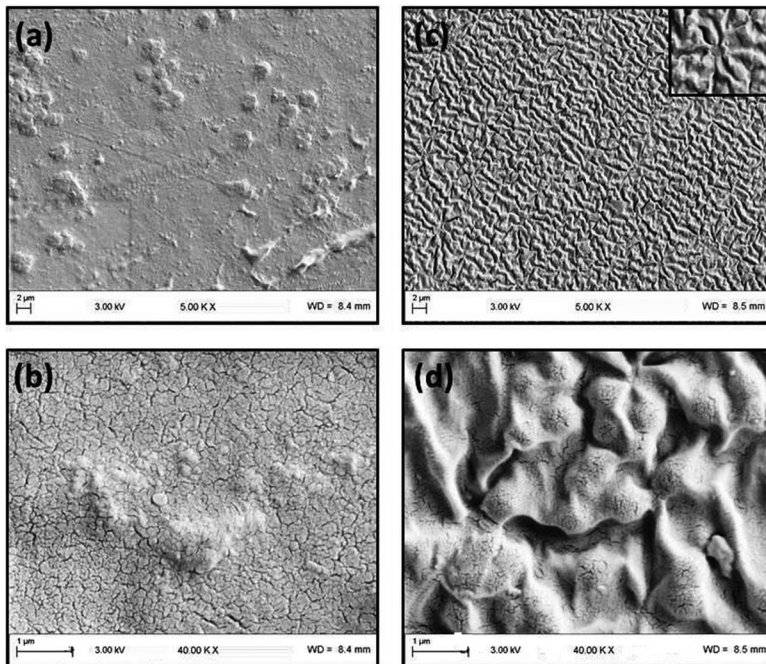


Figure 11: FESEM images for: (a) and (b) PVA-PANI polymer membrane, (c) and (d) PVA-PANI-BFO polymer-nanocomposite membrane at room temperature with different magnifications, respectively.

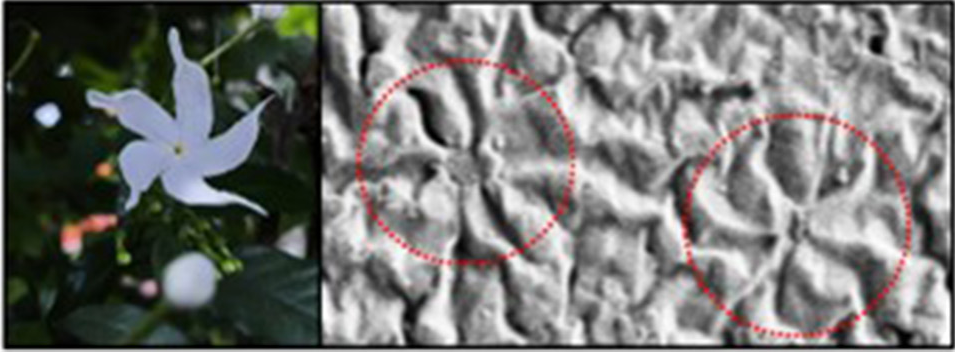


Figure 12: Structural growth of PVA-PANI-BFO polymer-nanocomposite membrane looks like the *Tabernaemontana divaricate* flower petal.

### 3.2 Weight Variation of the Synthesised Polymer Membranes with RH

The variations in weight and moisture intake percentage at different RH for the PVA-PANI and the PVA-PANI-BFO membranes are represented by the graphical plots in Figures 13(a) and (b). The moisture intake percentage of the PVA-PANI and the PVA-PANI-BFO membranes for absorption of moisture from the ambient can be calculated using the following equation:

$$W_m(\%) = \frac{W_f - W_i}{W_i} \times 100 \quad (10)$$

Where  $W_m$  is the moisture intake percentage by the membrane,  $W_f$  is the final weight of the membrane after moisture intake at a particular RH, and  $W_i$  is the initial weight of the membrane at a certain minimum RH of the ambient.<sup>50</sup> From those graphical representations, it is seen that at RH = 55%, the PVA-PANI-BFO membrane shows slightly higher weight gain with a little greater moisture intake percentage than the PVA-PANI membrane. On the contrary, at higher RH around and above RH = 80%, the PVA-PANI-BFO membrane shows a slightly lower weight gain with a lesser moisture uptake percentage relative to the PVA-PANI membrane. Finally, at RH = 95%, the PVA-PANI-BFO polymer-nanocomposite membrane clearly shows remarkably low weight increment, indicating a comparatively lower moisture intake percentage than the PVA-PANI polymer membrane. Thus, the BFO nanoparticle helps the polymer-nanocomposite membrane system to be stabilised more relative to the simple polymer membrane system against the ambient's RH.

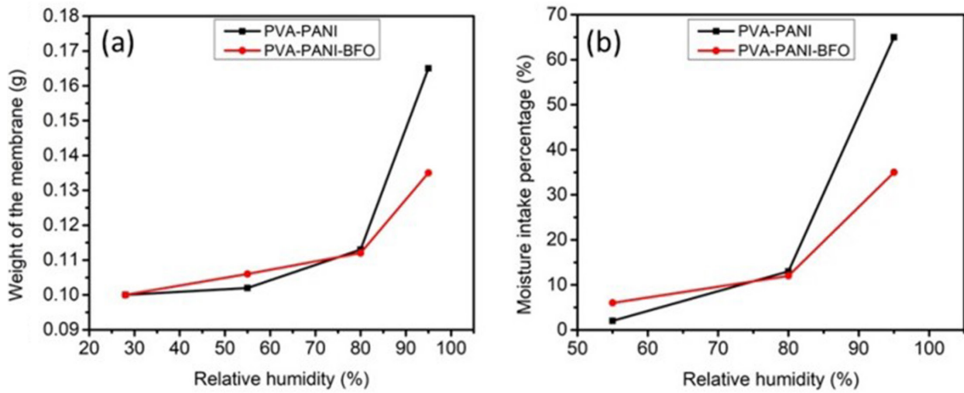


Figure 13: (a) Weight variation and (b) moisture intake percentage of PVA-PANI and PVA-PANI-BFO membranes at different RH.

### 3.3 Ionic Conductivity Measurement for the Synthesised PVA-PANI and PVA-PANI-BFO Membranes

The impedance of the RC equivalent system is naturally a complex quantity. This complex quantity consists of a real part ( $Z'$ ) and an imaginary part ( $Z''$ ). The plot of  $Z'$  versus  $Z''$  is known as the Nyquist plot or the Cole-Cole plot. This plot on a linear scale provides a semi-circle. The intercept of that semicircle on the real axis representing the real part of impedance towards the lower frequency site provides the bulk resistance ( $R$ ) of a membrane sandwiched between electrodes.<sup>51</sup> This bulk resistance ( $R$ ) helps to estimate the ionic conductivity of polymer or polymer-nanocomposite membranes. Figure 14 represents the Cole-Cole plots at different relative humidity for PVA-PANI polymer membrane and PVA-PANI-BFO polymer-nanocomposite membranes, respectively. The estimated bulk resistances for the PVA-PANI and the PVA-PANI-BFO membranes from Cole-Cole plots and the ionic conductivities of the respective membranes at different RH are represented in Table 1. With varying RH, the bulk resistance of any sample membrane is varied. As a result of which the ionic conductivity is changed.

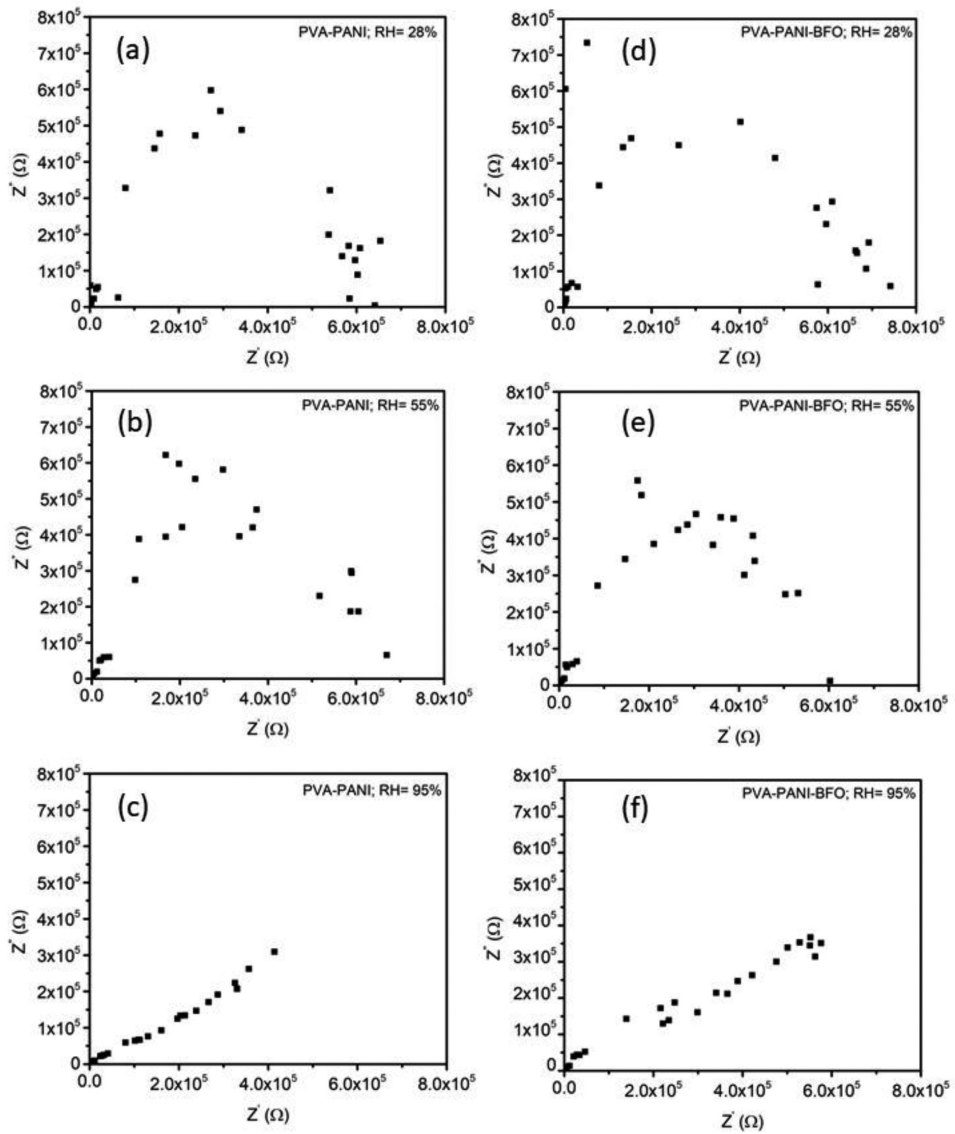


Figure 14: Variation of  $Z''$  (complex part of impedance) with  $Z'$  (real part of impedance) at (a) RH = 28%, (b) RH = 55%, (c) RH = 95% for PVA-PANI membrane and (d) RH = 28%, (e) RH = 55%, (f) RH = 95% for PVA-PANI-BFO membrane.

Table 1: The bulk resistances and ionic conductivities of PVA-PANI and PVA-PANI-BFO membranes estimated from Cole-Cole plots at different relative humidity

RH (%)	PVA-PANI membrane		PVA-PANI-BFO membrane	
	Bulk resistance (R in K $\Omega$ )	Ionic conductivity ( $\sigma$ in S/cm)	Bulk resistance (R in K $\Omega$ )	Ionic conductivity ( $\sigma$ in S/cm)
28	69.109	$3.646 \times 10^{-7}$	111.392	$1.795 \times 10^{-7}$
55	100.555	$2.506 \times 10^{-7}$	120.808	$1.655 \times 10^{-7}$
95	81.723	$3.083 \times 10^{-7}$	100.555	$1.988 \times 10^{-7}$

The variations in ionic conductivities for the PVA-PANI and PAV-PANI-BFO membranes at different RH are presented in Figure 15. With increasing the RH, from RH = 28% towards a maximum RH = 95%, the conductivity of PVA-PANI membrane decreases up to a certain threshold RH = 55%, then with further raising the RH (95%), ionic conductivity slightly increases again. Relatively, the PVA-PANI-BFO membrane does not exhibit such abrupt variation, where the plot is almost parallel to the horizontal axis that represents the RH. This plot indicates almost stable conductivity with the variation of RH. Besides this, it is seen that the PVA-PANI membrane has a comparatively higher ionic conductivity than PVA-PANI-BFO membranes at different RH. It indicates a greater moisture adsorption tendency by PVA-PANI membrane than PVA-PANI-BFO membrane. The BFO nanoparticles act as nanofiller in the polymer-nanocomposite membrane, play a vital role by preventing moisture adsorption from ambient and making the polymer composite system steadier.

Ionic conductivity depends on the number of free ions in the sample. Polyaniline makes easy ion absorption and accumulation in the membrane and enhances the electrical capacitance of the neighbouring electrode layer. Polyaniline consists of many cations, such as hydrogen ion ( $H^+$ ) or hydroxonium ions ( $H_3O^+$ ), which promote ionic conduction. They are comparatively very small-sized ions with higher mobility in the water ( $H_2O$ ) media, which get facility during penetration in the polymer membrane, where the thickness of the membrane does not affect the ionic transport.<sup>52</sup> In the appearance of  $H_2O$  molecules, protons ( $H^+$ ) are dissociated from the PVA-PANI structure and turn into highly mobile ions. Thus, due to the increase of proton mobility with the enhancement of  $H_2O$  molecules' adsorption (the increase of RH), the conductivity of a membrane increases. Besides this,  $H_2O$  molecules have some drawbacks that separate the polymeric chain, by which the conductivity of the membrane can decrease.<sup>53,54</sup> This phenomenon is observed at RH = 55% for the PVA-PANI membrane. Furthermore, the lower concentrations of BFO nanoparticles in any film exhibit a higher water contact angle ( $\approx 97^\circ$ ), which indicates the hydrophobic

nature.<sup>55</sup> That is why the lower concentration of BFO (2% weight) relative to PVA-PANI composite (95% weight) in the PVA-PANI-BFO polymer-nanocomposite membrane reflects the more hydrophobic nature in comparison to the PVA-PANI membrane. The hydrophobic nature of the BFO nanofiller drives the PVA-PANI-BFO membrane towards lesser moisture ( $H_2O$ ) adsorption than the PVA-PANI membrane. Therefore, at several RH, the synthesised PVA-PANI-BFO membrane exhibits a lower ionic conductivity than the synthesised PVA-PANI membrane. Also, the conductivity variation due to varying RH is very minimal for the PVA-PANI-BFO membrane relative to the PVA-PANI membrane.

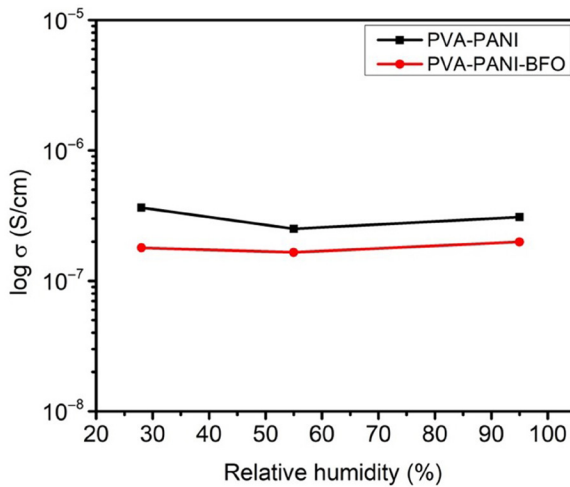


Figure 15: Variation of ionic conductivity with RH for PVA-PANI and PVA-PANI-BFO membranes.

#### 4. CONCLUSIONS

An environment-friendly synthesis process is implemented for synthesising BFO nanoparticles using the leaf extract of *Moringa oleifera* L. It is very infrequent to find preceding evidence of green synthesised BFO nanoparticles, particularly the synthesis using *Moringa oleifera* L. leaf extract. It is also very rare to evident the utilisation of green synthesised BFO nanoparticles as nanofiller to construct the PVA-PANI-BFO polymer-nanocomposite membrane. For the comparative study, the PVA-PANI and PVA-PANI-BFO membranes are made from the solution cast method. Individually PVA has no ionic conductivity, but the PANI as emeraldine base has conductivity in the order of  $10^{-7}$  S  $cm^{-1}$  that makes the synthesised membrane conductive. The RH of the

surroundings influences the conductive nature of synthesised membranes. The minimal concentration of BFO nanoparticles in the PVA-PANI-BFO membrane makes it slightly lower hydrophilic relative to the PVA-PANI membrane. This phenomenon is also reflected in the FTIR spectra in the range between  $3000\text{ cm}^{-1}$ – $4000\text{ cm}^{-1}$  for both the membranes at RH = 28% and RH = 95%. Thus, the PVA-PANI-BFO membrane shows lower ionic conductivity relative to the PVA-PANI membrane at various RH. The inclusion of BFO nanoparticles as nanofiller in the membrane makes it more stable against the surrounding humidity, which may have some advanced applications for electrochemical devices in the future in an open environment to overcome the negative impacts of moisture. Furthermore, the properties of the synthesised membranes relate to the change in ionic conductivity with the variation of RH, which can be useful for humidity sensing applications.

## 5. ACKNOWLEDGEMENTS

Author Mr. Diptarka Roy is very thankful to the University Grant Commission (UGC), Government of India (GOI), New Delhi, India, for the financial support to accomplish doctoral research work. We are thankful to Prof. K. N. Uttam, Department of Physics, University of Allahabad, for providing the Raman spectroscopy facility.

## 6. REFERENCES

1. Godara, S. et al. (2014). Combined structural, electrical, magnetic and optical characterization of bismuth ferrite nanoparticles synthesized by auto-combustion route. *J. Asian Ceram. Soci.*, 2(4), 416–421. <https://doi.org/10.1016/j.jascr.2014.09.001>
2. Chaturvedi, S. et al. (2014). Coercivity and exchange bias of bismuth ferrite nanoparticles isolated by polymer coating. *J. Appl. Phys.*, 115(12), 123906. <https://doi.org/10.1063/1.4869657>
3. Chen, G. et al. (2019). Bismuth ferrite materials for solar cells: Current status and prospects. *Mater. Res. Bullet.*, 110, 39–49. <https://doi.org/10.1016/j.materresbull.2018.10.011>
4. Biasotto, G. et al. (2011). Microwave-hydrothermal synthesis of perovskite bismuth ferrite nanoparticles. *Mater. Res. Bullet.*, 46(12), 2543–2547. <https://doi.org/10.1016/j.materresbull.2011.08.010>
5. Bajpai, O. P. et al. (2018). Magnetic properties and photocatalytic activity of bismuth ferrite nanoparticles grafted on graphene nanosheets. *New J. Chem.*, 42, 10712–10723. <https://doi.org/10.1039/C8NJ02030B>

6. Chakraborty, S. & Pal, M. (2018). Highly efficient novel carbon monoxide gas sensor based on bismuth ferrite nanoparticles for environmental monitoring. *New J. Chem.*, 42(9), 7188–7196. <https://doi.org/10.1039/C8NJ01237G>
7. Hu, Y. et al. (2011). Synthesis of bismuth ferrite nanoparticles via a wet chemical route at low temperature. *J. Nanomater.*, 2011(797639), 1–6. <https://doi.org/10.1155/2011/797639>
8. Rezaayat, M. et al. (2014). Green one-step synthesis of catalytically active palladium nanoparticles supported on cellulose nanocrystals. *ACS Sustainable Chem. Eng.*, 2(5), 1241–1250. <https://doi.org/10.1021/sc500079q>
9. Xia, B. et al. (2013). Preparation of bimetallic nanoparticles using a facile green synthesis method and their application. *Langmuir*, 29(15), 4901–4907. <https://doi.org/10.1021/la400355u>
10. Foidl, N. et al. (2001). The potential of *Moringa oleifera* for agricultural and industrial uses. In *International workshop, Dar Es Salaam, Tanzania, 20th October–2nd November 2001*, CIRAD, 2001. [https://moringatrees.org/moringa-doc/the\\_potential\\_of\\_moringa\\_oleifera\\_for\\_agricultural\\_and\\_industrial\\_uses.pdf](https://moringatrees.org/moringa-doc/the_potential_of_moringa_oleifera_for_agricultural_and_industrial_uses.pdf)
11. Li, S. et al. (1989). Synthesis and characterization of soluble polyaniline. *Synth. Met.*, 29(1), 329–336. [https://doi.org/10.1016/0379-6779\(89\)90314-7](https://doi.org/10.1016/0379-6779(89)90314-7)
12. Shacklette, L. W. & Han, C. C. (1993). Solubility and dispersion characteristics of polyaniline. *Mat. Res. Soc. Symp. Proc.*, 328, 157–166. <https://doi.org/10.1557/PROC-328-157>
13. Molapo, K. M. et al. (2012). Electronics of conjugated polymers (I): Polyaniline. *Int. J. Electrochem. Sci.*, 7, 11859–11875. <http://www.electrochemsci.org/papers/vol7/71211859.pdf>
14. Anju, V. P. & Narayanankutty, S. K. (2016). Polyaniline coated cellulose fiber/ polyvinyl alcohol composites with high dielectric permittivity and low percolation threshold. *AIP Advanc.*, 6(015109), 1–13. <https://doi.org/10.1063/1.4940664>
15. Osman, Z. et al. (2001). Conductivity enhancement due to ion dissociation in plasticized chitosan based polymer electrolytes. *Carbohydr. Poly.*, 44(2), 167–173. [https://doi.org/10.1016/S0144-8617\(00\)00236-8](https://doi.org/10.1016/S0144-8617(00)00236-8)
16. Baskaran, R. et al. (2004). Dielectric and conductivity relaxations in PVAc based polymer electrolytes. *Ionics*, 10, 129–134. <https://doi.org/10.1007/BF02410321>
17. Achenbach, G. D. et al. (1967). Preparation of single-phase polycrystalline  $\text{BiFeO}_3$ . *J. Am. Ceram. Soc.*, 50(8), 437–437. <https://doi.org/10.1111/j.1151-2916.1967.tb15153.x>
18. Langford, J. I. & Wilson, A. J. C. (1978). Seherrer after sixty years: A survey and some new results in the determination. *J. Appl. Cryst.*, 11, 102–113. <https://doi.org/10.1107/S0021889878012844>
19. Ghosh, S. et al. (2005). Low temperature synthesis of bismuth ferrite nanoparticles by a ferrioxalate precursor method. *Mater. Res. Bull.*, 40, 2073–2079, <https://doi.org/10.1016/j.materresbull.2005.07.017>

20. Patel, A. K. et al. (2014). On the crystallinity of PVA/palm leaf biocomposite using DSC and XRD techniques. *Microsyst Technol.*, 20, 41–49. <https://doi.org/10.1007/s00542-013-1882-0>
21. Sanches, E. A. et al. (2014). Nanostructured polyaniline emeraldine-base form (EB-PANI): A structural investigation for different neutralization times. *J. Molecul. Struct.*, 1074, 732–737. <https://doi.org/10.1016/j.molstruc.2014.05.046>
22. Bousalem, S. et al. (2020). Physical and electrochemical investigations on hybrid materials synthesized by polyaniline with various amounts of ZnO nanoparticle. *Chem. Phys. Lett.*, 741(137095), 1–6. <https://doi.org/10.1016/j.cplett.2020.137095>
23. Khozemey, E. E. et al. (2020). Radiation synthesis of gas sensor based on polyaniline nanoflake-poly vinyl alcohol film for four hazardous gases (NH<sub>3</sub>, CO<sub>2</sub>, H<sub>2</sub>S and phenol). *Arab J. Nucl. Sci. Appl.*, 53(3), 210–221. <https://doi.org/10.21608/ajnsa.2020.20000.1302>
24. Pakalniškis, A. et al. (2020). Nanoscale ferroelectricity in pseudo-cubic sol-gel derived barium titanate - bismuth ferrite (BaTiO<sub>3</sub>-BiFeO<sub>3</sub>) solid solutions. *J. Alloy. Comp.*, 830(154632), 1–7. <https://doi.org/10.1016/j.jallcom.2020.154632>
25. Soam, A., et al. (2020). Development of paper-based flexible supercapacitor: Bismuth ferrite/graphene nanocomposite as an active electrode material. *J. Alloys Comp.* 813(152145), 1–9. <https://doi.org/10.1016/j.jallcom.2019.152145>
26. Verma, R. et al. (2021). Effect of calcination temperature on structural and morphological properties of bismuth ferrite nanoparticles. *Ceram. Int.*, 47(3), 3680–3691. <https://doi.org/10.1016/j.ceramint.2020.09.220>
27. Palai, R. et al. (2008). Polarized Raman scattering of multiferroic BiFeO<sub>3</sub> single domain crystal and thin film. Paper presented at the 17<sup>th</sup> IEEE International Symposium on the Applications of Ferroelectrics, Santa Re, NM, USA, 23–28 February 2008, 1–4. <https://doi.org/10.1109/ISAF.2008.4693780>
28. Li, W. et al. (2020). Flexible Poly(vinyl alcohol)-Polyaniline hydrogel film with vertically aligned channels for an integrated and self-healable supercapacitor. *ACS Appl. Energy Mater.*, 3(9), 9408–9416. <https://doi.org/10.1021/acsam.0c01794>
29. Li, L. et al. (2020). Cryopolymerization enables anisotropic polyaniline hybrid hydrogels with superelasticity and highly deformation-tolerant electrochemical energy storage. *Nature Communicat.*, 11(62), 1–12. <https://doi.org/10.1038/s41467-019-13959-9>
30. Wang, Y. et al. (2020). An all-in-one supercapacitor with high stretchability via a facile strategy. *J. Mater. Chem. A*, 8(17), 8255–8261. <https://doi.org/10.1039/D0TA00757A>
31. Wang, J. et al. (2020). Facile synthesis of multi-functional elastic polyaniline/polyvinyl alcohol composite gels by a solution assembly method. *RSC Adv.*, 10(37), 22019–22026. <https://doi.org/10.1039/d0ra02238a>
32. Zarach, Z. et al. (2020). Improving the performance of a graphite foil/polyaniline electrode material by a thin PEDOT: PSS layer for application in flexible, high power supercapacitors. *Materials*, 13(24), 5791. <https://doi.org/10.3390/ma13245791>

33. Cooney, T. F. et al. (1994). Raman spectral study of solid and dissolved poly(vinyl alcohol) and ethylene-vinyl alcohol copolymer. *J. Polym. Sci.: Part B: Polym. Phys.*, 32(7), 1163–1174. <https://doi.org/10.1002/polb.1994.090320704>
34. Okechukwu, V. U. et al. (2021). Evaluation of phytochemical constituents of methanol extract of *Moringa oleifera* Lam. whole leaf by gas chromatography-mass spectrometry and fourier transform infrared spectroscopy analysis. *World News Natur. Sci.*, 37, 18–30. <http://psjd.icm.edu.pl/psjd/element/bwmeta1.element.psjd-1d212a55-3a40-4356-b593-fc503c9dcf73>
35. Letsholathebe, D. et al. (2021). Green synthesis of ZnO doped *Moringa oleifera* leaf extract using Tiron yellow dye for photocatalytic applications. *Mater. Today: Proceed.*, 36(2), 475–479. <https://doi.org/10.1016/j.matpr.2020.05.119>
36. Hassabo, A. G. et al. (2020). Multifarious cellulosic through innovation of highly sustainable composites based on Moringa and other natural precursors. *Int. J. Biologic. Macromol.*, 165 (A), 141–155. <https://doi.org/10.1016/j.ijbiomac.2020.09.125>
37. Tovar, G. I. et al. (2020). Biogenic synthesis of iron oxide nanoparticles using *Moringa oleifera* and chitosan and its evaluation on corn germination. *Environ. Nanotechnol. Monit. Manag.*, 14, 100350. <https://doi.org/10.1016/j.enmm.2020.100350>
38. Mhamad, S. A. et al. (2020). Rapid synthesis of pure phase bismuth ferrite through modified sol-gel auto-ignition method: Impact of different chelating agents. *ChemistrySelect*, 5(43), 13584–13590. <https://doi.org/10.1002/slct.202002827>
39. Sakar, M. et al. (2013). Annealing temperature mediated physical properties of bismuth ferrite (BiFeO<sub>3</sub>) nanostructures synthesized by a novel wet chemical method. *Mater. Res. Bull.*, 48(8), 2878–2885. <https://doi.org/10.1016/j.materresbull.2013.04.008>
40. Prabhakaran, T. & Hemalatha, J. (2012). Negative giant magnetoresistance effect in single layered superparamagnetic polymer nanocomposite structures of poly(vinyl alcohol)–polyaniline/bismuth ferrite. *Smart Mater. Struct.*, 21, 085012. <https://doi.org/10.1088/0964-1726/21/8/085012>
41. Atta, A. et al. (2021). Flexible methyl cellulose/polyaniline/silver composite films with enhanced linear and nonlinear optical properties. *Polymers*, 13(8), 1225. <https://doi.org/10.3390/polym13081225>
42. Joo, H. et al. (2020). Fabrication of poly(vinyl alcohol)-polyaniline nanofiber/graphene hydrogel for high-performance coin cell supercapacitor. *Polymers*, 12(4), 928. <https://doi.org/10.3390/polym12040928>
43. Zhao, Y. et al. (2020). Hierarchically structured stretchable conductive hydrogels for high-performance wearable strain sensors and supercapacitors. *Matter*, 3(4), 1196–1210. <https://doi.org/10.1016/j.matt.2020.08.024>
44. Hamed, M. G. & Hassan, A. A. (2020). Enhancement of the structural and optical properties of (PVA-PANI) polymer blend by addition of CuI

- nanoparticles. *IOP Conf. Series: Mater. Sci. Eng.*, 928(072157), 1–13. <https://doi.org/10.1088/1757-899X/928/7/072157>
45. Zhou, H. et al. (2021). Capacitive pressure sensors containing reliefs on solution-processable hydrogel electrodes. *ACS Appl. Mater. Interfaces*, 13(1), 1441–1451. <https://doi.org/10.1021/acsami.0c18355>
  46. Mojet, B. L. et al. (2010). Light at the interface: The potential of attenuated total reflection infrared spectroscopy for understanding heterogeneous catalysis in water. *Chem. Soc. Rev.*, 39(12), 4643–4655. <https://doi.org/10.1039/c0cs00014k>
  47. Lai, F. et al. (2020). Self-healing flexible and strong hydrogel nanocomposites based on polyaniline for supercapacitors. *Ionics*, 26, 3015–3025. <https://doi.org/10.1007/s11581-020-03438-3>
  48. Nandiyanto, A. B. D. & Ragadhita, R. O. R. (2019). How to read and interpret FTIR spectroscopy of organic material. *Indonesian J. Sci. Technol.*, 4(1), 97–118. <https://doi.org/10.17509/ijost.v4i1.15806>
  49. Huafeng, Z. et al. (2011). Preparation and characterization of PVDF hydrophobic membrane. *Adv. Mater. Res.*, 221, 338–342. <https://doi.org/10.4028/www.scientific.net/AMR.221.338>
  50. Mishra, A. K. et al. (2012). Silicate-based polymer-nanocomposite membranes for polymer electrolyte membrane fuel cells. *Prog. Polym. Sci.* 37(6), 842– 869. <https://doi.org/10.1016/j.progpolymsci.2011.11.002>
  51. El-Nahass, M. M. et al. (2014). Electrical conductivity and dielectric measurements of CoMTPP. *Mater. Chem. Phys.*, 143(2), 490–494. <https://doi.org/10.1016/j.matchemphys.2013.08.038>
  52. Chulkin, P. & Łapkowski, M. (2020). An insight into ionic conductivity of polyaniline thin films. *Materials*, 13(12), 1–21. <https://doi.org/10.3390/ma13122877>
  53. De, S. et al. (2011). Humidity dependence of the ionic conductivity of polyelectrolyte complexes. *Macromolecules*, 44(22), 8936–8943. <https://doi.org/10.1021/ma201949s>
  54. Wang, H., et al. (2015). Ionic Seebeck effect in conducting polymers. *Adv. Energy Mater.*, 5(11), 1500044. <https://doi.org/10.1002/aenm.201500044>
  55. Mane, P. V. et al. (2019). Bismuth ferrite thin film as an efficient electrode for photocatalytic degradation of Methylene blue dye. *Mater. Res. Exp.*, 6(2), 026426. <https://doi.org/10.1088/2053-1591/aaf096>